Sensors and Actuators A 220 (2014) 213–220

Contents lists available at ScienceDirect

Sensors and Actuators A: Physical

journal homepage: www.elsevier.com/locate/sna

High-performance infrared photo-transistor based on SWCNT decorated with PbS nanoparticles

Mohsen Asad[a,*], Morteza Fathipour[b], Mohammad Hossein Sheikhi[a], Mahdi Pourfath[b,c]

[a] School of Electrical and Computer Engineering, Shiraz University, 71345-1585 Shiraz, Iran
[b] School of Electrical and Computer Engineering, University of Tehran, 14395-515 Tehran, Iran
[c] Institute for Microelectronics, TU Wien, Gusshausstrasse 27-29/E360, 1040 Vienna, Austria

ARTICLE INFO

Article history:
Received 31 May 2014
Received in revised form 13 October 2014
Accepted 14 October 2014
Available online 23 October 2014

Keywords:
Photo-transistor
Fast switching
Nanotube
Lead sulfide nanoparticles
Transport characteristics

ABSTRACT

This paper presents a low-cost high-gain infrared photo-transistor based on a nano-heterostructure comprising of a single wall carbon nanotube (SWCNT) decorated with PbS nanoparticles (NPs). These structures are prepared using a solution based process with chemical bonding of PbS NPs on SWCNT walls. SWCNT act as an efficient electron transfer channel from PbS NPs to electrodes. By optimization the band alignment between PbS NPs and the SWCNTs fast transfer of electrons is achieved. Fabricated photo-transistor exhibits a relatively fast response with an enhanced sensitivity up to 35% under a laser illumination with a wavelength of 1550 nm and a power intensity of about 2 mW/cm^2. Conversion from p-type to n-type operation is obtained by changing the polarity of the gate voltage. High gain, excellent on/off photo-current ratio and stable operation indicate potential application of SWCNT as a charge extraction strategy.

1. Introduction

Fabrication of semiconductor nanoparticles (NPs) on matrices of functional materials has been extensively studied for optoelectronic applications [1–4]. To enhance the external quantum efficiency, it is essential to extract the photo-generated electron–hole carriers faster than their recombination lifetime. This requires the use of efficient electron pathways from the matrices toward the electrodes. Such a carrier-collecting pathway has been demonstrated for various matrix templates such as conductive polymer films and carbon nanotubes (CNTs) [5–7]. It has been shown that the combination of semiconducting NPs, such as CdSe, as the photosensitive element, and conjugated conductive polymers as the matrix benefits from the advantages of these two classes of materials [8]. While conjugated polymers are efficient channels for transport of excitons, inorganic NP energy bands can be tuned by modifying its dimension and morphology for forming an efficient infrared photocell. However, conjugated polymers suffer from relatively low carrier mobility. In contrast, the superior electrical conductivity of CNTs renders them as excellent materials for conductive matrices [9]. Due to their unique properties, CNTs have been extensively used in different chemical compositions for a wide variety of applications [10–14]. Several research groups have investigated photoconductivity of SWCNTs [15–18] as well as for multi-wall CNTs (MWCNTs) [19]. However, SWCNTs are generally more promising because of their higher performance in terms of charge-carrier mobility and stability in ambient conditions [20,21].

Developing highly efficient near-infrared (IR) photo-transistors is challenging. On the one hand, various types of inorganic NPs have shown great promise for this spectrum, because of the tunability of the absorption wavelength with the geometry of NPs [22–24]. On the other hand, colloidal method for fabricating II–IV compound quantum dots (QDs) has attracted much attention due to its simple and well-established solution based synthesis. In particular, strong photo-absorption in the near-IR spectral region is reported in colloidal PbS QD-based photoconductors [25,26] and photodiodes [27–29]. Due to their optical and physical properties, PbS QDs have already been employed for fabricating displays [30] and solar cells [31]. Efficient charge extraction from colloidal NPs, however, remains a challenge.

In this paper, we combine the advantages of nanoclusters (NCs) of PbS NPs and SWCNTs by conjugating them into a nano-heterostructure (NH) matrix that can be used in thin film optical devices. Photo-transistors based on SWCNT-PbS NPs are developed using a simple and cost-effective wet chemical process. We present an efficient fabrication method for decorating of SWCNT sidewalls with PbS NPs, using a chemical reduction process in deionized (DI)

* Corresponding author at: School of Electrical and Computer Engineering, Shiraz University, Zand Street, Shiraz, Iran. Tel.: +98 711 628 6421; fax: +98 711 628 6421.
E-mail address: mohsenasad@shirazu.ac.ir (M. Asad).

http://dx.doi.org/10.1016/j.sna.2014.10.017
0924-4247/

water medium. This decoration process induces strong chemical bonding between PbS NPs and SWCNTs, which facilitates efficient carrier transport through NH matrices.

2. Experimental setup

2.1. Preparation of SWCNT/PbS NCs

Surface functionalization prepares CNT wall surfaces for efficient bonding with other materials. An essential approach to form a highly functionalized surface is creating active sites on CNT walls [32,33]. Highly concentrated PbS NPs are employed for covalent bonding to SWCNTs. In the SWCNT-PbS NPs heterostructure photogenerated carries at the PbS photosensitive NPs are transferred to SWCNTs through which they can be easily absorbed by electrodes. The processes of functionalization and decoration of SWCNTs is illustrated schematically in Fig. 1.

SWCNTs (with outer diameter ~10 nm, length ~20 μm, purity 95%) are provided by Parsis Co., Iran. For the functionalization of SWCNT surface, they are dispersed in H_2SO_4 and HNO_3 (1:3) and mixed at 120 °C for 2 h. The mixture is left overnight. The functionalized SWCNTs are then filtered and rinsed using DI water and dried at 60 °C in a vacuum oven for 6 h. This process leads to the formation of active sites that are negatively charged which in turn facilitate chemical bonds.

Lead acetate ($Pb(CH_3COOH)$) and Tiore (NH_2CSNH_2) from Merck, Germany are employed as sources of lead and sulfur, respectively, for PbS NPs. To decorate PbS NPs onto functionalized SWCNT walls, 30 mg of dried functionalized SWCNTs are dispersed in 50 ml DI water and sonicated for 30 min followed by stirring at 70 °C for 10 min. Thereafter, 30 mg of lead acetate is added and stirred for another 15 min while the solution turned from black to gray. Following this process Pb^{2+} ions are reduced and deposited on the functionalized sites of SWCNT walls which are negatively charged. Next, 20 mg of Tiore is added to the solution followed by stirring for 3 h, after which it completely turned dark. After cooling down, the final powder is filtered and rinsed using DI water.

Functionalization process, however, can break π-bonding symmetry of sp^2-hybridized orbitals and can lead to the formation of defects over the CNT walls [34]. These defects increase the recombination sites at SWCNTs and reducing carrier lifetime which is detrimental for photo-detection applications. Employing hydrogen passivation, many defects can be annealed and carrier lifetime can be significantly enhanced. Annealing of powder is carried out in the presence of hydrogen at 60 °C for 1 h.

2.2. Device fabrication

The polyethylene terephthalate (PET) is used as the flexible substrates. Aluminum (Al) electrodes with a length of 200 μm and a width of 6000 μm are evaporated on the PET substrate and then patterned by lift-off lithography (Fig. 2a). The fabrication processes is shown schematically in Fig. 2b. SWCNT-PbS NPs are dispersed in 50 ml dimethylformamide (DMF) and the suspension is spun onto the substrates (PET with patterned Al electrodes) at 4000 rpm for 30 s in air, followed by thermal annealing for 10 min at 90 °C in N_2. The film deposition cycle is carried out multiple times in order to obtain different SWCNT-PbS NPs film thicknesses for the further investigation. The schematic of the fabricated device is shown in Fig. 2c. The initial thickness of the resulting NH thin film is about 70 nm.

2.3. Characterization

Vibrational, rotational and low-frequency modes of SWCNTs before and after functionalization are characterized by Raman spectroscopy. Samples morphology is analyzed using field emission scanning electron microscopy (FE-SEM, Hitachi S4160) and the elemental structure is analyzed using Zeiss EVO40 SEM equipped with an energy dispersive X-ray detector (EDX, EDAX Oxford, UK). X-ray diffraction (XRD) patterns are collected using a Philips XPert Pro Model with illumination source with a wavelength of $\lambda = 1.54$ nm at 2θ angels between 10° and 90°. The absorption spectra of prepared NH are obtained using a Frontier NIR Perkin Elmer system. Current–voltage (JV) characteristics are obtained using an HP 4145 semiconductor parameter analyzer under IR irradiation at 1550 nm, using standard GaAs laser diode.

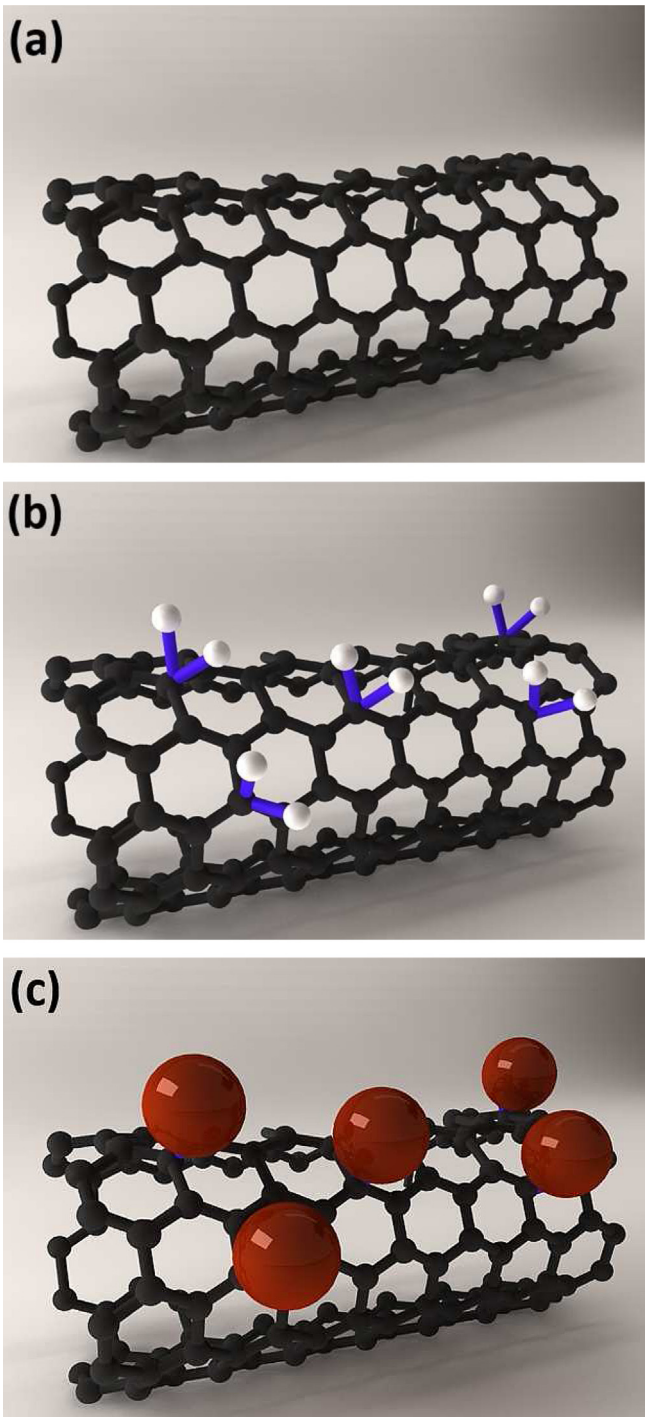

Fig. 1. The schematic of SWCNT decoration with PbS NPs. (a) Pristine SWCNT, (b) surface functionalization using acid treatment, and (c) decoration of SWCNT sidewalls with PbS NPs by wet chemical process.

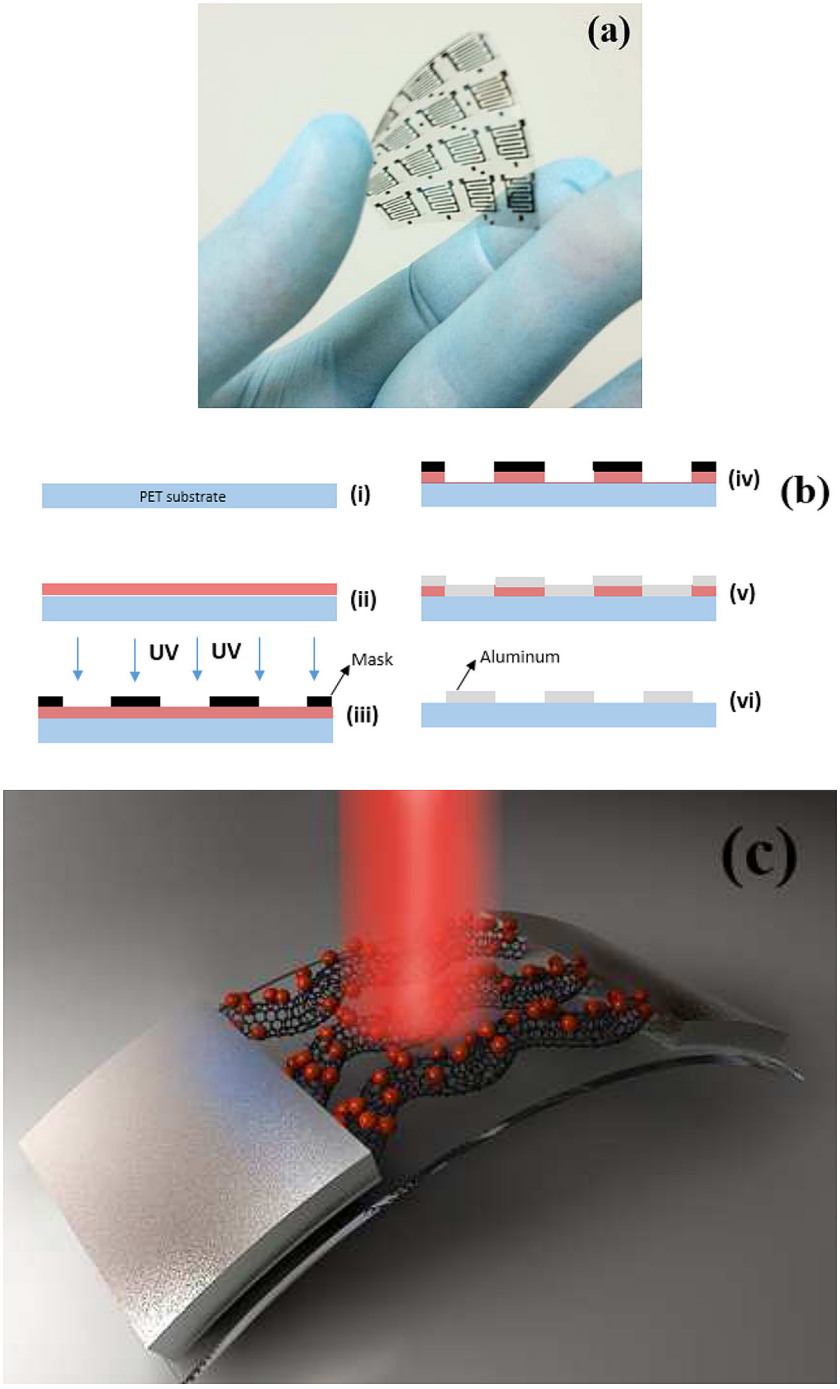

Fig. 2. (a) A photograph of the fabricated electrodes on the flexible PET substrate and (b) schematic of fabrication process. (i) Bare PET substrate, (ii) AZ3007 photoresist is coated on the substrate at 1000/3000 rpm and then backed at 95 °C for 2 min. The achieved thickness is 1.7 μm, (iii) photoresist is patterned using conventional i-line photolithography system, (iv) the exposed photoresist is eliminated by development process using AZ400 developer, (v) 1 μm aluminum layer is deposited on the patterned surface using sputtering system (Nanostructure Coating Co., Iran), (vi) IDTs form by lift-off in acetone. (c) Schematic of the NP-decorated CNT device.

3. Results and discussion

3.1. Raman spectroscopy

As can be seen from Fig. 3a, the G band is originated from the Raman active mode of graphene at 1579 cm^{-1}. Fig. 3b shows a displacement in G band to 1582 cm^{-1} after the functionalization. The intensity of the D band, which is generated by the in-plane transverse optical phonon mode, is a measure of the defect concentration along the tube [35]. A comparison of intensity ratio of D/G bands (I_D/I_G) shown in Fig. 3a and b illustrates that after SWCNTs functionalization, the defect concentration increases. The Raman spectrum of SWCNTs decorated with PbS NPs is shown in Fig. 3c. PbS shows Raman peaks at 160, 206 and 308 cm^{-1} corresponding to one longitudinal optical phonon, two-phonon processes, and two longitudinal phonon modes, respectively [36,37]. The peak at 837 cm^{-1} is related to photo-degradation of PbS and is perhaps due to one of the $PbSO_4$, $PbO–PbSO_4$, $3PbO–PbSO_4$ and $4PbO–PbSO_4$ products. Further shift in the G band of SWCNTs can be seen for the PbS NPs decorated SWCNTs which is due to charge transfer between PbS NPs and SWCNTs surfaces.

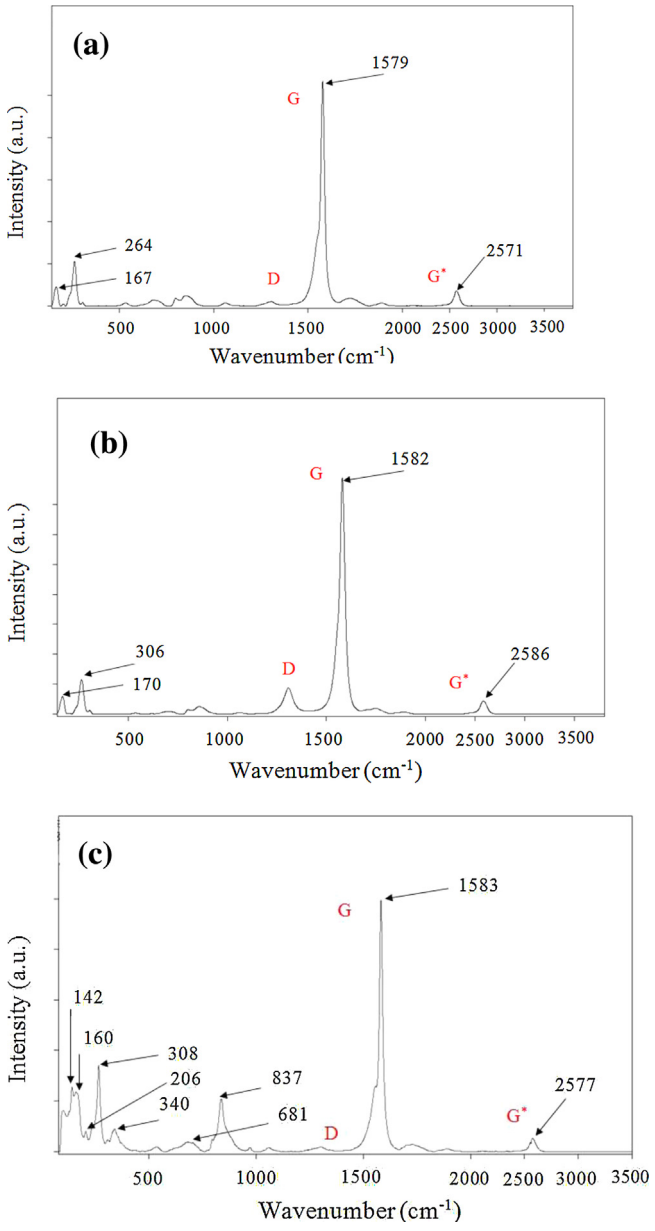

Fig. 3. Raman spectrum of SWCNTs: (a) before acid treatment, (b) after acid treatment, and (c) after PbS NPs formation.

In the low frequency region, the spectrum is dominated by the in-phase mode known as radial breathing mode (RBM), see Fig. 3a. The frequency of the RBM is inversely proportional to the nanotube diameter (d_t) [38] $\omega_{RBM} = A/d_t$, where the proportionality constant (A) is an empirically determined parameter equal to 234 nm/cm. Therefore, the Raman peak shifts at 167 and 264 cm^{-1} in Fig. 3a correspond to SWCNTs with diameters of 1.58 nm and 0.89 nm, respectively.

3.2. Morphological study and EDS analysis

The morphological structure of the SWCNTs-PbS NPs NH is investigated using SEM imaging. As shown in Fig. 4a and b, the matrix is made of bundles of SWCNTs covered with cubic shaped PbS NPs. The elemental composition of the PbS-SWCNT matrix is obtained using EDS (Fig. 4c). The qualitative and quantitative analyses have been used to find out what elements in which relativity exists in our prepared NH. By performing qualitative analysis, each

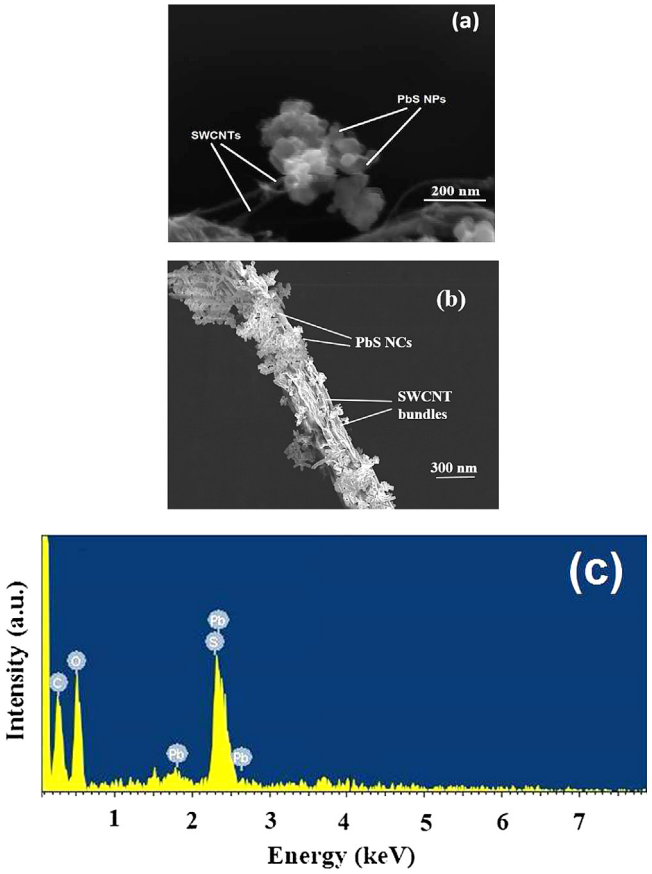

Fig. 4. (a) and (b) The SEM images of SWCNTs decorated with PbS NPs. (c) EDS analysis of SWCNT-PbS NPs heterostructure.

element has to identify according to specific energy of the characteristic X-ray peak. Considering the fact that the mass of the element penetrated by the incident electron is approximately constant regardless of composition, the relative intensity of an X-ray line is approximately proportional to the mass concentration of the element concerned. In our research, a Pb to S peak ratio was obtained about 1.03 from Fig. 4c, which indicates excellent PbS stoichiometry.

3.3. Structural analysis

XRD pattern of pristine SWCNTs (without PbS NPs) is illustrated in Fig. 5a. This pattern shows peaks of (1 0 0) and (0 0 2) which are related to the graphite phase (NO 41-1487, JCPDS card file). Fig. 5b shows XRD pattern of SWCNT-PbS NPs heterostructure. The remaining diffraction peaks are consistent with (2 0 0), (1 1 1), (2 2 0), (3 1 1), (2 2 2), (4 0 0), (3 3 1), (4 2 0), and (4 2 2) according to card file NO JCPDC-5-592. They belong to PbS nanoclusters faced centered cubic phase of PbS, confirming that perfectly crystalline nanocrystals are synthesized onto SWCNTs.

3.4. Optical absorption

Absorption spectrum of SWCNT-PbS NPs heterostructure over the wavelength range 700–3500 nm is depicted in Fig. 6. Due to one-dimensional van Hove singularities absorption spectrum peaks at certain energies [39]. Fabricated SWCNTs are identified as semiconductor, because E_{11}, which corresponds to the first interband transition, and E_{22} absorption peaks appear at 950 nm and 1700 nm, respectively [40–42]. However, E_{22} is overshadowed the by presence of the predominant PbS peak for light absorption.

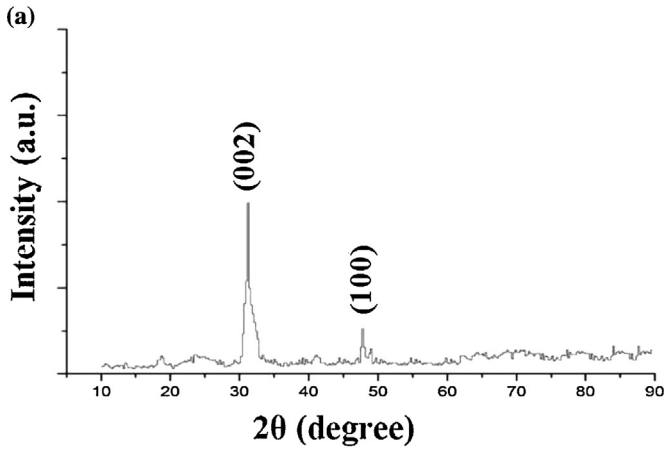

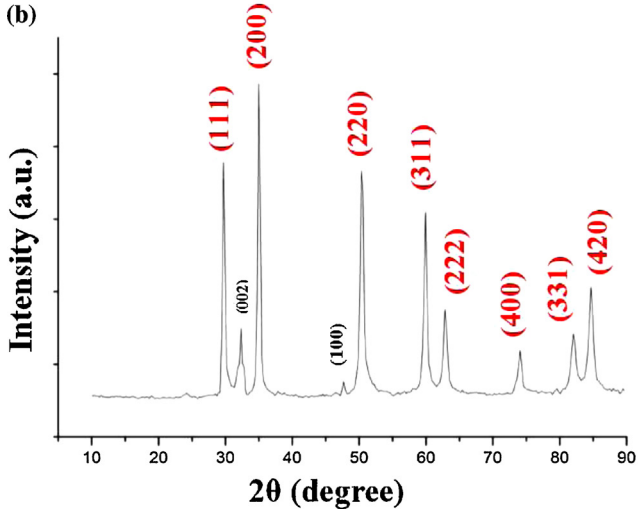

Fig. 5. XRD patterns of (a) pristine SWCNT and (b) SWCNT-PbS NPs heterostructure.

Another peak is also observed at 2000 nm that reveals the SWCNT-PbS NPs heterostructure has a significant absorption in the near-IR.

The photo harvesting mechanism is carried out by the absorption of photons with energies equal or larger than the band gap of NPs which produce electron–hole. The characteristics of SWCNT-PbS NPs heterostructure strongly depend on the band alignment between the SWCNTs and the NPs. The conduction band (CB) and the valence band (VB) energy levels of the PbS NPs have been reported to be at 3.5 eV and 4.9 eV, respectively and the

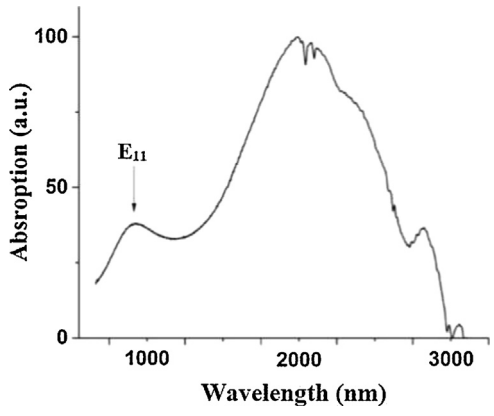

Fig. 6. Optical absorption spectrum of SWCNT-PbS NPs heterostructure.

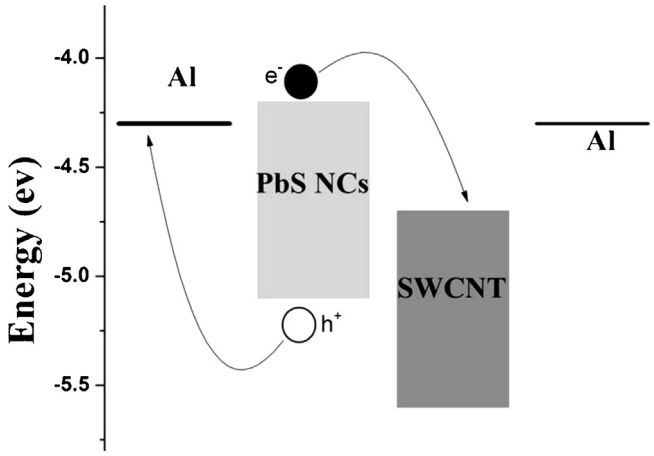

Fig. 7. Energy band diagram of SWCNT-PbS NPs heterostructure.

highest occupied molecular orbital (HOMO) and the lowest unoccupied molecular orbital (LUMO) of the SWCNT is known to be 4.7 eV and 5.6 eV, respectively [39]. Due to lower position of the Fermi level of SWCNTs with respect to the CB of PbS, electron injection from CB of photo-excited PbS NPs into SWCNTs is energetically favorable. A photo-generated electron (e^-) in the CB of PbS NPs is transferred to SWCNT whereas a photo-generated hole (h^+) in the VB of PbS is transferred directly to the electrode (Fig. 7). Transferred electrons to the SWCNT are absorbed by the electrodes within a transit time τ_{tr} which is much shorter than the recombination lifetime τ_{gr} in PbS. This leads to a faster photoresponse of SWCNT-PbS NPs than PbS NPs.

3.5. Photoresponse characterization

The photoresponse of SWCNT-PbS NPs heterostructure is characterized under dark and under illumination conditions using standard laser diode at 1550 nm. The resistance of the devices is measured as an output characteristic of the device, employing an HP 4145B semiconductor parameter analyzer at room temperature. The distance of the IR diode and device is appropriately selected to obtain an incident power of 2 mW/cm^2 on the surface of phototransistor.

Fig. 8a compares the photoresponse of the SWCNT-PbS NPs heterostructure as a function of the film thickness with that of the pristine SWCNTs. Relative photo-resistance modulation of 3% and 35% under 1550 nm illumination are obtained for a 70 nm thick pristine SWCNT and a 70 nm thick SWCNT-PbS NPs respectively. This indicates that the main cause for the photo-resistance modulation in the SWCNT-PbS NPs heterostructure is the charge transfer from NPs to SWCNT. Achieving such a high photo-response is an evidence for the coupling between PbS NPs and SWCNTs. Regardless of the thickness of the film, negligible photo-resistance modulations are observed by pristine SWCNT-based In contrast the photoresponse of the SWCNT-PbS NPs heterostructure is found to exhibit a dependence upon the prepared film thickness. For thicker films, a higher photo-response is achieved, because PbS sites increase and hence photo-excited carriers increase consequently.

Fig. 8b shows typical switching response of SWCNT-PbS NPs heterostructure at $V_{DS} = 5$ V and $V_{GS} = 0$ V and under laser illumination with a wavelength of 1550 nm. Fabricated devices exhibit a very reproducible response under repeated on–off cycles of the laser diode. The decay time is about 10 ms which is significantly shorter than 200 s that is reported by Li et al. for SWCNT-CdS NPs system [43]. This is perhaps due to the fact that chemical bonds between CdS NPs and SWCNTs were not optimized in their work. The response time of CNT-QDs heterostructure has been improved

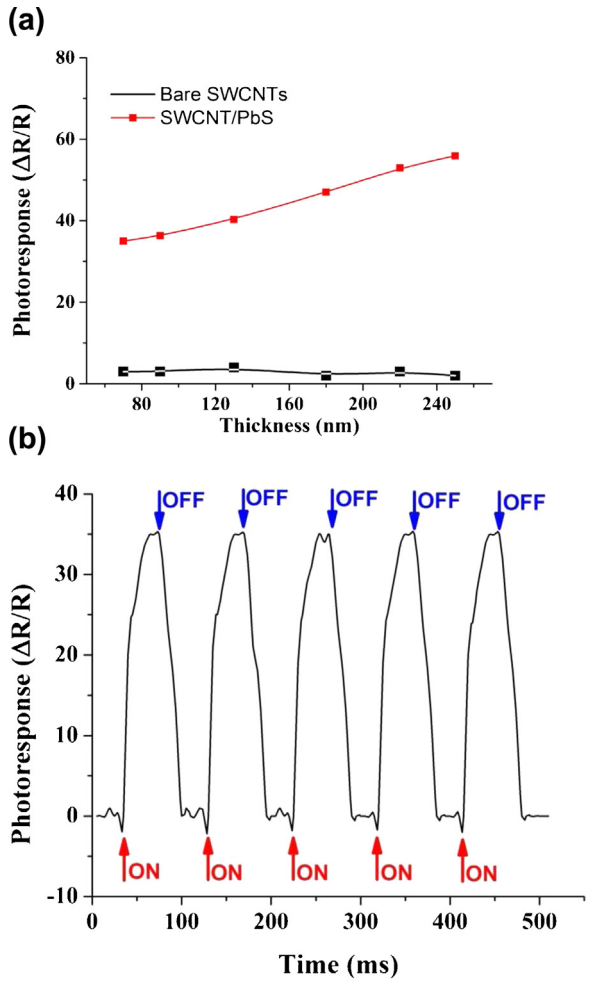

Fig. 8. (a) The photo-response of the SWCNT/PbS as a function of the film thickness. (b) Response time of devices at V_{DS} = 5 V upon illumination of 1550 nm and 2 mW/cm^2 light intensity.

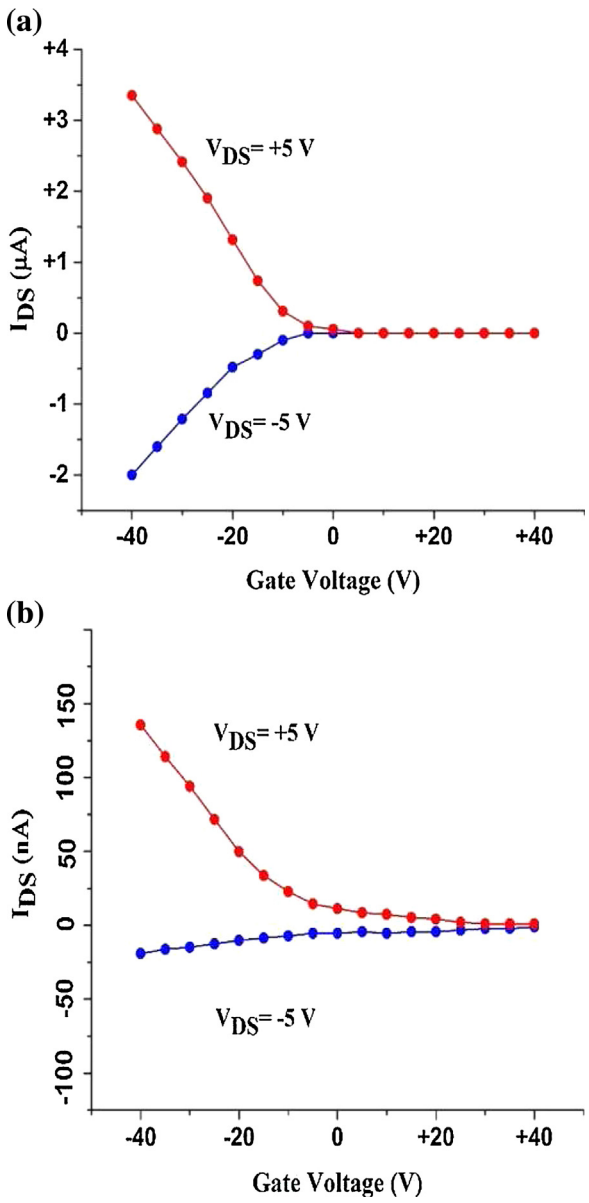

Fig. 9. Transport characteristics of SWCNT FET at dark condition (a) before PbS decoration and (b) after decoration with PbS NPs and dried at 90 °C in N_2.

to 10 s by Shim et al. using two-step dielectrophoresis (DEP) of CNT and QDs. Methods based on employing organic linkers in the NH also result in relatively long response times [44]. This suggests that use of SWCNT results in a relatively fast charge transport due to stronger chemical bonding between SWCNT and PbS NPs.

3.6. Transport characterization

As mentioned earlier, SWCNTs are used as efficient channels for collecting photo-generated charge carriers from semiconducting PbS NPs. To characterize carrier transport in SWCNTs, a back gate configuration based on SiO_2 over silicon is used. Thickness of SiO_2 layer is about 300 nm and electrodes are patterned using lift-off lithography on the SiO_2 surface. Fig. 9a presents the transfer characteristics of pristine SWCNT-FET as a function of V_{GS} at $V_{DS} = -5$ V and $V_{DS} = +5$ V. Apparently, pristine SWCNT-FETs show p-type operation. As shown in Fig. 9b, the SWCNT-PbS NPs based FETs show also p-type behavior, but with a smaller drain-source current (I_{DS}). Troutman et al. have reported an equation for current per unit width, $K = I_D/W = \mu_g Q_n V_D/L$ [45], where μ_g is the effective mobility for carriers in SWCNT and Q_n is the area charge density. The reduction of I_{DS} can be due to the change in the magnitude of charge density because of NPs and formation of scattering sites by NPs along the SWCNT.

To investigate transport characteristics, type conversion of SWCNT-PbS FET is facilitated by changing the polarity of the gate voltage under dark and illuminated condition. Fig. 10a and b shows that I_{DS} is about 10 nA for a positive gate voltage whereas it is about 160 nA for a negative gate voltage. The decrease of I_{DS} for positive gate voltages clearly indicates that electrons are the main photo-generated carriers that are transferred from PbS NPs to SWCNTs. Photo-generated electrons can be transferred from PbS NPs to hole rich (p-type) SWCNT and recombine with holes, thus the conductivity and current are reduced. At negative gate voltages, however, the Fermi-level of the SWCNT approaches the CB of PbS NPs which makes SWCNT an n-type channel and electrons become majority carriers in the channel which results in the reduction of carrier recombination and as a result the enhancement of conductivity and current. The generated holes also remain in the NPs and contributed in the enhancement of the conductivity as a positive electric field that support electron transferring from the contacts to the channel. These transport characteristics validate our proposed model on energy band alignment (Fig. 7).

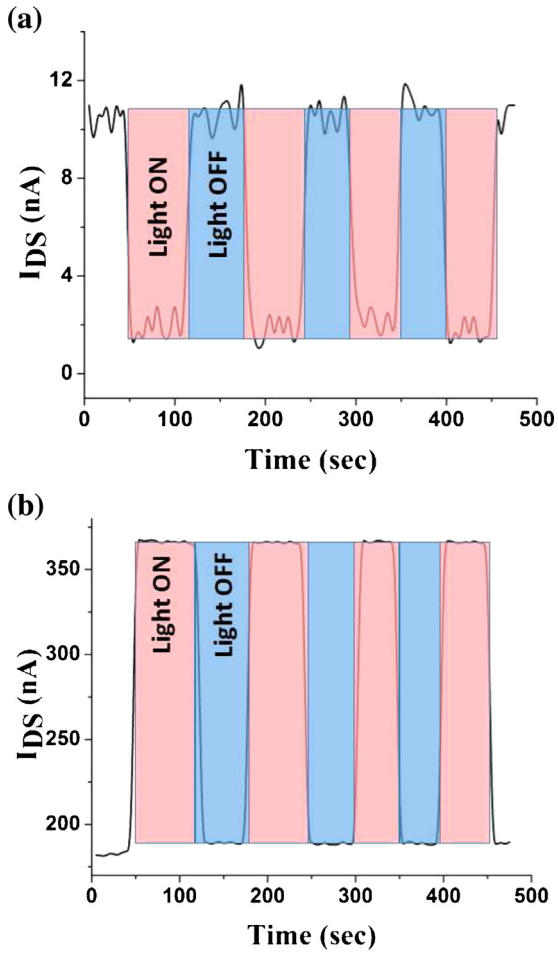

Fig. 10. Modulation of the drain-source current under laser illumination with a wavelength of 1550 nm and a power density of about 2 mW/cm^2 (a) at V_{GS} = +40 V and (b) V_{GS} = −40 V. V_{DS} = 5 V for all experiments.

4. Conclusion

Enhanced photo-transistor which consists of SWCNTs decorated with PbS NPs is reported in this work. SWCNTs act as electron transfer channel and PbS NPs act as photon harvesting components for this system. This allows photo-generation and detection in the near-IR spectrum range. Raman, SEM, EDS, and XRD experiment are carried out to demonstrate PbS NPs are chemically bonded to SWCNTs walls and electronic interaction between PbS and SWCNTs exists. Significant improvement in the response time of transient photo-current is observed. Employing type conversion strategy, the transferred charge carriers are demonstrated to be electrons. The results show that SWCNTs-PbS NPs heterostructures are promising candidates for future optoelectronic applications.

Acknowledgement

We acknowledge valuable discussions and analyzing RAMAN spectrum by Prof. Kourosh Kalantar-zadeh from School of Electrical Engineering, Royal Melbourne Institute of Technology.

References

[1] S. Barenjee, S.S. Wong, Synthesis and characterization of carbon nanotube-nanocrystal heterostructures, Nano Lett. 2 (2002) 195–200.
[2] S. Ravindran, S. Chaudhary, B. Colburn, M. Ozkan, C.S. Ozkan, Covalent coupling of quantum dots to multiwalled carbon nanotubes for electronic device applications, Nano Lett. 3 (2003) 447–453.
[3] Q. Huang, L. Gao, Synthesis and characterization of CdS/multiwalled carbon nanotube heterojunctions, Nanotechnology 15 (2004) 1855.
[4] E. Granot, F. Patolsky, I. Wilner, Electrochemical assembly of a CdS semiconductor nanoparticle monolayer on surfaces: structural properties and photoelectrochemical applications, J. Phys. Chem. B 108 (2004) 5875–5881.
[5] I. Robel, B.A. Bunker, P.V. Kamat, Single-walled carbon nanotube–CdS nanocomposites as light-harvesting assemblies: photoinduced charge-transfer interactions, Adv. Mater. 17 (2005) 2458–2463.
[6] L. Sheeney-Haj-Ichia, J. Wasserman, I. Willner, CdS-nanoparticle architectures on electrodes for enhanced photocurrent generation, Adv. Mater. 14 (2002) 1323–1326.
[7] L. Sheeney-Haj-Ichia, B. Basnar, I. Willner, Efficient generation of photocurrents by using CdS/carbon nanotube assemblies on electrodes, Angew. Chem. Int. Ed. 44 (2005) 78–83.
[8] W.U. Huynh, J.J. Dittmer, A.P. Alivisatos, Hybrid nanorod-polymer solar cells, Science 295 (2004) 2425–2427.
[9] Y. Liao, Ch. Zhang, X. Wang, X.G. Li, S.J. Ippolito, K. Kalantar-zadeh, R.B. Kaner, Carrier mobility of single-walled carbon nanotube-reinforced polyaniline nanofibers, J. Phys. Chem. C. 115 (2011) 16187–16192.
[10] M. Asad, M.H. Sheikhi, Surface acoustic wave based H_2S gas sensors incorporating sensitive layers of single wall carbon nanotubes decorated with Cu nanoparticles, Sens. Actuators B: Chem. 194 (2014) 134–141.
[11] R. Andrews, D. Jacques, D. Qian, T. Rantell, Multiwall carbon nanotubes: synthesis and application, Acc. Chem. Res. 35 (2002) 1008–1017.
[12] R.H. Baughman, A.A. Zakhidov, W.A. Heer, Carbon nanotubes – the route toward applications, Science 297 (2002) 787–792.
[13] S. Lu, Y. Liu, N. Shao, B. Panchapakesan, Nanotube micro-opto-mechanical systems, Nanotechnology 18 (2007) 065501.
[14] C. Li, Y. Liu, X. Huang, H. Jiang, Direct sun-driven artificial heliotropism for solar energy harvesting based on a photo-thermomechanical liquid-crystal elastomer nanocomposite, Adv. Funct. Mater. 22 (2012) 5166–5174.
[15] A. Fujiwara, Y. Matsuoka, H. Suematsu, N. Ogawa, K. Miyano, H. Kataura, Y. Maniwa, Sh. Suzuki, Y. Achiba, Photoconductivity in semiconducting single-walled carbon nanotubes, Jpn. J. Appl. Phys. 40 (2001) L1229–L1231.
[16] I.A. Levitsky, W.B. Euler, Photoconductivity of single-wall carbon nanotubes under continuous-wave near-infrared illumination, Appl. Phys. Lett. 83 (2003) 1857–1859.
[17] S. Lu, B. Panchapakesan, Photoconductivity in single wall carbon nanotube sheets, Nanotechnology 17 (2006) 1843–1850.
[18] Y. Liu, S. Lu, B. Panchapakesan, Alignment enhanced photoconductivity in single wall carbon nanotube films, Nanotechnology 20 (2009) 035203.
[19] L. Liu, Y. Zhang, Multi-wall carbon nanotube as a new infrared detected material, Sens. Actuators A 116 (2004) 394–397.
[20] C. Dekker, Carbon nanotubes as molecular quantum wires, Phys. Today 52 (1999) 22–28.
[21] F. Kreupl, A.P. Graham, G.S. Duesberg, W. Steinhogl, U.M.E. Leibau, W. Honlein, Carbon nanotubes in interconnect applications, Microelectron. Eng. 64 (2002) 399–408.
[22] J.M. Pietryga, R.D. Schaller, D. Werder, M.H. Stewart, V.I. Klimov, J.A. Hollingsworth, Pushing the band gap envelope: mid-infrared emitting colloidal PbSe quantum dots, J. Am. Chem. Soc. 126 (2004) 11752–11753.
[23] M.V. Kovalenko, D.V. Talapin, M.A. Loi, F. Cordella, G. Hesser, M.I. Bodnarchuk, W. Heiss, Quasi-seeded growth of ligand-tailored PbSe nanocrystals through cation-exchange-mediated nucleation, Angew. Chem. Int. Ed. 47 (2008) 3029–3033.
[24] E. Lifshitz, M. Brumer, A. Kigel, A. Sashchiuk, M. Bashouti, M. Sirota, E. Galun, Z. Burshtein, A.Q.L. Quang, I. Ledoux-Rak, J. Zyss, Air-stable PbSe/PbS and PbSe/$PbSe_xS_{1-x}$ core–shell nanocrystal quantum dots and their applications, J. Phys. Chem. B 110 (2006) 25356–25365.
[25] G. Konstantatos, I. Howard, A. Fischer, S. Hoogland, J. Clifford, E. Klem, L. Levina, E.H. Sargent, Ultrasensitive solution-cast quantum dot photodetectors, Nature 442 (2006) 180–183.
[26] G. Konstantatos, E.H. Sargent, Nanostructured materials for photon detection, Nat. Nanotechnol. 5 (2010) 391–400.
[27] E.H. Sargent, Infrared photovoltaics made by solution processing, Nat. Photonics 3 (2009) 325–331.
[28] K. Szendrei, F. Cordella, M.V. Kovalenko, M. Böberl, G. Hesser, M. Yarema, D. Jarzab, O.V. Mikhnenko, A. Gocalinska, M. Saba, F. Quochi, A. Mura, G. Bongiovanni, P.W.M. Blom, W. Heiss, M.A. Loi, Solution-processable near-IR photodetectors based on electron transfer from PbS nanocrystals to fullerene derivatives, Adv. Mater. 21 (2009) 683–687.
[29] T.P. Osedach, N. Zhao, S.M. Geyer, L. Chang, D.D. Wanger, A.C. Arango, M.C. Bawendi, V. Bulović, Interfacial recombination for fast operation of a planar organic/QD infrared photodetector, Adv. Mater. 22 (2010) 5250–5254.
[30] P. Yang, C.F. Song, M.K. Lu, X. Yin, G.J. Zhou, D. Xu, D.R. Yuana, The luminescence of PbS nanoparticles embedded in sol–gel silica glass, Chem. Phys. Lett. 345 (2001) 429–434.
[31] P.K. Nair, M.T.S. Nair, PbS solar control coatings: safety, cost and optimisation, J. Phys. D: Appl. Phys. 23 (1990) 150–155.
[32] D.W.H. Fam, A.I.Y. Tok, A. Palaniappan, P. Nopphawan, A. Lohani, S.G. Mhaisalkar, Selective sensing of hydrogen sulphide using silver nanoparticle decorated carbon nanotubes, Sens. Actuators B 138 (2009) 189–192.
[33] K. Dai, L. Shi, J. Fang, Y. Zhang, Synthesis of silver nanoparticles on functional multi-walled carbon nanotubes, Mater. Sci. Eng. A 465 (2007) 283–286.
[34] N.G. Sahoo, S. Rana, J.W. Cho, L. Li, S.H. Chan, Polymer nanocomposites based on functionalized carbon nanotubes, Prog. Polym. Sci. 35 (2010) 837–867.

[35] A. Jorio, G. Dresselhaus, M.S. Dresselhaus, M. Souza, M.S.S. Dantas, M.A. Pimenta, A.M. Rao, R. Saito, C. Liu, H.M. Cheng, Polarized Raman study of single-wall semiconducting carbon nanotubes, Phys. Rev. Lett. 85 (2000) 2617–2620.
[36] T.D. Krauss, F.W. Wise, D.B. Tanner, Observation of coupled vibrational modes of a semiconductor nanocrystal, Phys. Rev. Lett. 76 (1996) 1376–1379.
[37] K.K. Nanda, S.N. Sahu, R.K. Soni, S. Tripathy, Raman spectroscopy of PbS nanocrystalline semiconductors, Phys. Rev. B 58 (1998) 15405–15407.
[38] A. Jorio, R. Saito, J.H. Hafner, C.M. Lieber, M. Hunter, T. McClure, G. Dresselhaus, M.S. Dresselhaus, Structural (n,m) determination of isolated single-wall carbon nanotubes by resonant Raman scattering, Phys. Rev. Lett. 86 (2001) 1118–1121.
[39] H. Kataura, Y. Kumazawa, Y. Maniwa, I. Umezu, S. Suzuki, Y. Ohtsuka, Y. Achiba, Optical properties of single-wall carbon nanotubes, Synth. Met. 103 (1999) 2555–2558.
[40] S.M. Bachilo, M.S. Strano, C. Kittrell, R.H. Hauge, R.E. Smalley, R.B. Weisman, Structure-assigned optical spectra of single-walled carbon nanotube, Science 298 (2002) 2361–2366.
[41] M.E. Itkis, S. Niyogi, M.E. Meng, M.A. Hamon, H. Hu, R.C. Haddon, Spectroscopic study of the Fermi level electronic structure of single-walled carbon nanotubes, Nano Lett. 2 (2002) 155–159.
[42] I. Ka, V. Le Borgne, D. Ma, M.A. El Khakani, Pulsed laser ablation based direct synthesis of single-wall carbon nanotube/PbS quantum dot nanohybrids exhibiting strong, spectrally wide and fast photoresponse, Adv. Mater. 47 (2012) 6289–6294.
[43] X. Li, Y. Jia, A. Cao, Tailored single-walled carbon nanotube-CdS nanoparticle hybrids for tunable optoelectronic devices, ACS Nano 4 (2010) 506–512.
[44] H.C. Shim, S. Jeong, C-S. Han, Controlled assembly of CdSe/MWNT hybrid material and its fast photoresponse with wavelength selectivity, Nanotechnology 22 (2011) 165201.
[45] R.R. Troutman, A. Kotwal, A device model for the amorphous-silicon staggered-electrode thin-film transistor, IEEE Trans. Electron Devices 36 (1989) 2915–2922.

Biographies

Mohsen Asad is a Ph.D. candidate and research assistant at the School of Electrical and Computer Engineering, Shiraz University, Iran. He has been worked about three years at MEMS & NEMS Lab under supervisory of Prof. Fathipour at University of Tehran, Iran. Then he moved to Nanotechnology Research Institute at Shiraz University. His research interests include developing process and fabricating prototype innovative sensors and optoelectronic devices based on semiconductor science and physics of quantum materials.

Morteza Fathipour received his M.S. and Ph.D. degrees in solid-state electronics from Colorado State University, Fort Collins, in 1980 and 1984, respectively. From 1984 to 1986, he was with Sharif University of Technology, Tehran, Iran. He then joined the Department of Electrical and Computer Engineering, University of Tehran, Tehran, where he is the Founder of the Technology Computer-Aided Design (CAD) Laboratory. His research interests include device physics, semiconductor interface, process/device design, simulation, modeling and characterization for Ultra Large Scale Integration (ULSI) devices, CAD development for process and device design, fabrication of nanodevices, and optoelectronics.

Mohammad Hossein Sheikhi received his B.Sc. (1994) degree in electrical engineering from Shiraz University, Shiraz, Iran, the M.Sc. (1996) degree from Sharif University of Technology, Tehran, Iran and the Ph.D. degree in electrical engineering from Tarbiat Modarres University, Tehran in 2000. Dr. Sheikhi was selected as the distinguished PhD student graduated from Tarbiat Modarres University in 2000. He joined Tohokou University, Sendai, Japan, as a Research Scientist in 2000. After joining Shiraz University in 2001, he focused on the optoelectronics, nanosensors, and nanotransistors. He is currently the Associate Professor and Head of Nanotechnology Research Institute (NRI), Shiraz University, Shiraz, Iran.

Mahdi Pourfath was born in Tehran, Iran, in 1978. He received the B.S and M.S. degrees in electrical engineering from Sharif University of Technology, Tehran, in 2000 and 2002, respectively, and the Ph.D. degree in Microelectronics from the Technische Universität Wien, Austria, in 2007. He has authored or co-authored over 100 scientific publications and presentations and authored one monograph. He is now an Assistant Professor in the School of Electrical and Computer Engineering, University of Tehran. He is also with the institute of Microelectronics, Technische Universität Wien, Austria. His scientific interests include novel nanoelectronic devices and materials.